THE ASTRONOMICAL JOURNAL, 122:1938–1953, 2001 October

A DRAO AND VLA INVESTIGATION OF THE ENVIRONMENT OF WR 130

S. CICHOWOLSKI
Instituto Argentino de Radioastronomía, C.C. 5, 1894 Villa Elisa, Argentina; and Département de Physique and Observatoire du Mont Mégantic, Université Laval, Ste-Foy, Québec, G1K 7P4, Canada; silvina@phy.ulaval.ca

S. PINEAULT
Département de Physique and Observatoire du Mont Mégantic, Université Laval, Ste-Foy, Québec, G1K 7P4, Canada; pineault@phy.ulaval.ca

E. M. ARNAL
Instituto Argentino de Radioastronomía, C.C. 5, 1894 Villa Elisa, Argentina; and Facultad de Ciencias Astronómicas y Geofísicas, Universidad Nacional de La Plata, 1900 La Plata, Argentina; arnal@iar.unlp.edu.ar

J. C. TESTORI
Instituto Argentino de Radioastronomía, C.C. 5, 1894 Villa Elisa, Argentina; jtestori@iar.unlp.edu.ar

W. M. GOSS
National Radio Astronomy Observatory, P.O. Box O, Socorro, NM 87801; mgoss@aoc.nrao.edu

AND

C. E. CAPPA
Instituto Argentino de Radioastronomía, C.C. 5, 1894 Villa Elisa, Argentina; and Facultad de Ciencias Astronómicas y Geofísicas, Universidad Nacional de La Plata, 1900 La Plata, Argentina; ccappa@iar.unlp.edu.ar
Received 2001 March 30; accepted 2001 June 13

ABSTRACT

The environment of the Wolf-Rayet (WR) star WR 130 has been studied using the 21 cm H I line and radio continuum data at 408 and 1420 MHz obtained with the Dominion Radio Astrophysical Observatory (DRAO) Synthesis Telescope. In addition, the H110α recombination line and 21 cm H I line were observed using the Very Large Array in the DnC and D configurations. The Sharpless H II region, Sh 98 (size $\sim 15'$), and two OB stars are observed near the Wolf-Rayet star position. An extended ring-shaped structure (G68.1+1.1) of size $\sim 20'$ is observed in the radio continuum and infrared data. Of four compact radio sources seen superposed on the ring, one is an H II region of size $\sim 3'$ (G68.14+0.92), while the others are probably extragalactic. The spectral index ($S_\nu \propto \nu^\alpha$) of G68.1+1.1 is $\alpha = 0.0 \pm 0.1$. The thermal nature of G68.1+1.1 is confirmed by an analysis of the correlation between the brightness temperature at 21 cm and the brightness at 60 μm, as observed with *IRAS*. The DRAO H I data show an H I bubble in the velocity range -12 to 1 km s^{-1}. The most striking characteristic of the H I cavity is the excellent correlation with the radio continuum ring. The WR star is not at the center of the ring, but in the dense border to the east. This eccentric position can be explained by a combination of a high spatial velocity for the star and projection effects. The possible contribution of the OB stars present in the area is also considered. From our H110α observations, together with other recombination lines observed in the area, we deduce a distance of 12 kpc for the compact H II region G68.14+0.92 and 5 kpc for G68.1+1.1. We conclude that G68.1+1.1 is the radio counterpart of the optical H II region Sh 98, while G68.14+0.92 is a chance superposition of a much more distant source. The ionized mass of the ring is estimated at $\sim 3000\ M_\odot$ and the rms electron density at ~ 3 cm^{-3}, assuming a homogeneous distribution. A missing H I mass of 500 $M_\odot$ is obtained for the cavity and an excess H I mass of 1500 $M_\odot$ for the shell.

Key words: H II regions — infrared radiation — ISM: bubbles — ISM: H I — stars: individual (WR 130) — stars: Wolf-Rayet

1. INTRODUCTION

Massive O stars and their descendants are responsible for most of the spectacular phenomena occurring in the interstellar medium (ISM) in galaxies. These stars emit most of their light in the ultraviolet, giving rise to H II regions, and have extremely powerful winds that deposit large amounts of momentum and mechanical energy into the ISM that, over their lifetime, are comparable to those injected into the ISM by supernova explosions (see, e.g., Lozinskaya 1992 for a review).

The strong wind from a massive star sweeps up the ambient gas forming an interstellar bubble (IB) that has a double shock structure (Castor, McCray, & Weaver 1975). The inner shock stops the freely expanding wind, while the outer one sweeps up the ISM and forms a thin, radiatively cooled shell of swept-up gas. The hot shocked wind is separated from the swept-up ISM gas by a contact discontinuity. The entire bubble's dynamics depend on the nature of the inner shock. If this shock is radiative, then the momentum of the wind drives the expansion of the swept-up shell (Avedisova 1972; Steigman, Strittmater, & Williams 1975). In the opposite case, a region of hot shocked winds forms, and its thermal pressure ultimately drives the outer shell (Castor et al. 1975; Weaver et al. 1977).

Wolf-Rayet (WR) stars are believed to be evolved massive stars. Main-sequence stars having a mass in the range 25–40 $M_\odot$ evolve to WR stars after experiencing a red supergiant (RSG) phase (Maeder 1990). Since the wind speed and mass-loss rate differ significantly among the different evolution-

ary phases, there will be a variety of structures in the ISM local to WR stars (García-Segura & Mac Low 1995).

At the end of the WR phase, the star will explode as a supernova, and the supernova remnant (SNR) that forms after the explosion of the star will evolve within the highly complex ISM mentioned above. Certainly, the action of the WR star and its progenitors upon the ISM will have an impact on the evolution and appearance of the SNR (Brighenti & D'Ercole 1994, and references therein).

Since an IB is characterized by a low volume density, its signature will be a minimum in the brightness temperature of the observed H I distribution, as observed in the 21 cm H I line. If the star is at rest or has a low velocity with respect to the ISM and the ambient ISM is homogeneous, this cavity should be roughly centered at the position of the star and should be observed within a velocity range centered at a radial velocity that is characteristic of the local ISM.

In this paper, one in a series dealing with high angular H I studies of the properties of the ISM located toward O-type stars or their descendants, we report a 1420 MHz (line plus continuum) and 408 MHz (continuum) high-resolution study carried out using the Synthesis Telescope (ST) of the Dominion Radio Astrophysical Observatory (DRAO) toward the star WR 130 ($\equiv$LS 16), located at the position (J2000) $19^h59^m12^s.68$, $+31°27'9''.7$ or $(l, b) = (68°.22, +0°.98)$ (van der Hucht 2001). We also report observations of the 21 cm H I and H110α lines performed with the Very Large Array (VLA) of the National Radio Astronomy Observatory (NRAO).

WR 130 is classified as a WN8(h) star (van der Hucht 2001). The stellar distance is somewhat uncertain. Hidayat, Supelli, & van der Hucht (1982) suggest a distance of 4.9 kpc, while 4.8 kpc is quoted by van der Hucht et al. (1988). Using line-free spectrophotometric magnitudes and colors, a distance of 2.6 kpc is suggested by Conti & Vacca (1990). After a revision of the absolute magnitude scale, a distance of 2.7 kpc is given in the Seventh Catalogue of Galactic Wolf-Rayet Stars (van der Hucht 2001). The visual extinction of this star is about $A_V \simeq 6$ mag (van der Hucht 2001).

Based on 4.9 GHz continuum observations, Abbott et al. (1986) estimated an upper limit of $2.3 \times 10^{-5}\ M_\odot\ \mathrm{yr}^{-1}$ for the mass-loss rate. A terminal velocity, v_∞, of 1000 km s^{-1} was also derived (Willis 1991; Hamann, Koesterke, & Wessolowski 1995).

Using narrowband Hα emission-line imagery, Heckathorn, Bruhweiler, & Gull (1982) found a faint and diffuse 12′ diameter nebula that they suggest is a "shell structure probably related" to WR 130. This nebulosity is almost coincident with the Sharpless H II region Sh 98, which was classified as a circular, amorphous, and faint Hα nebulosity of size $\sim$15′ (Sharpless 1959). The positional coincidence between Sh 98 and WR 130 appears in the different catalogs of WR stars under the heading "correlation with H II region" (see, e.g., Table 13B of van der Hucht 2001), but no real physical association is implied. Based on interference filter CCD imagery in Hα and [O III] λ5007, Miller & Chu (1993) suggest that WR 130 lies "in nebulosity" without further comments.

2. OBSERVATIONS AND DATA REDUCTION

WR 130 was observed on 1999 April and May, with the DRAO ST operating simultaneously at 408 and 1420 MHz in continuum mode and at 1420 MHz in spectral line mode (H I). The telescope consists of seven 9 m antennas aligned on a 600 m east-west baseline (Landecker et al. 2000). All spacings from a minimum of 12.9 m were observed. Table 1 shows the instrumental parameters for the DRAO observations.

The reduction of continuum data from the ST followed conventional lines, including the application of CLEAN and self-calibration algorithms, and position and flux density registrations, as described in detail by Pineault & Joncas (2000). For the H I data, because of the almost complete coverage of the *u-v* plane, the sidelobe levels of the unCLEANed beam are low, and it was not necessary to

TABLE 1

DRAO ST Observational Parameters

Parameters	408 MHz	1420 MHz
Right ascension of the field center (J2000)	19 59 18	19 59 18
Declination of the field center (J2000)	31 27 30	31 27 30
Calibrators and assumed flux densities[a]	...	...
3C 147 (Jy)	48	21.3
3C 295 (Jy)	54	...
Received polarization	Right circular	Left circular
Field of view (to 50%) (deg)	5.3	1.7
Grating ring radii (deg)	9.8	2.8
Continuum:		
Bandwidth (MHz)[b]	3.5	30
Synthesized beam (EW × NS) (arcmin)	3.3 × 6.5	1.0 × 1.9
Observed rms noise (K)	0.65	0.02
H I spectral line:		
Synthesized beam (EW × NS) (arcmin)	...	1.0 × 1.9
Observed rms noise (single channel) (K)	...	1.5
Channel width (km s^{-1})	...	1.6
Velocity resolution (km s^{-1})	...	2.6
Velocity coverage (km s^{-1})	...	+170 to −250

Note.—Units of right ascension are hours, minutes, and seconds, and units of declination are degrees, arcminutes, and arcseconds.

[a] Flux densities on the scale of Baars et al. 1977.

[b] The 1420 MHz continuum bandpass excludes H I emission.

CLEAN the H I maps. The 128 H I images were inspected, and channels free of H I emission were averaged to form a continuum image that was then subtracted from each channel image to remove continuum emission. All images shown have had the continuum removed, and the velocities are with respect to the local standard of rest (LSR). Finally, because the DRAO ST cannot observe baselines shorter than 12.9 m, single-antenna observations were used to provide information on large-scale structure. For the continuum, the 1420 MHz Effelsberg survey (Kallas & Reich 1980) and 408 MHz all-sky survey from Haslam et al. (1982) were used. For the H I line maps, low-resolution images were obtained with the 26 m DRAO telescope. A detailed description of the spatial filtering process used to add the low-resolution information to the interferometric observations can be found in Joncas & Higgs (1990) or Normandeau, Taylor, & Dewdney (1997).

The region near WR 130 was also observed with the VLA in the D array for periods of 29 and 110.5 minutes on 1999 April 13 and 21, respectively, at a frequency of 4.87 GHz (H110α). In addition, on 2000 July 3, 2000 July 19, and 2000 August 13, observations in the 21 cm H I line were carried out using the VLA in the DnC (July 3) and D array. The instrumental parameters for all these observations are summarized in Table 2. All data editing, calibration, and imaging were performed using the AIPS software package.

To analyze the dust distribution, we obtained infrared images in the form of high-resolution–processed (HIRES; Fowler & Aumann 1994) *IRAS* images. The 60 and 100 μm images are part of the *IRAS* Galaxy Atlas produced by Cao et al. (1997) at the Infrared Processing and Analysis Center (IPAC).[1] The 12 and 25 μm Mid-Infrared Galaxy Atlas images were processed by Kerton & Martin (2000). The images used are the result of 20 iterations of the algorithm, giving an approximate resolution ranging from about 0.5 at 12 μm to about 2′ at 100 μm.

We also examined continuum data of this region obtained at 327, 2695, 4850, and 8350 MHz. These data were extracted from surveys carried out using the Westerbork Synthesis Radio Telescope (WSRT; Taylor et al. 1996), the 100 m Effelsberg Radio Telescope (Fürst et al. 1990), the NRAO Green Bank Radio Telescope (Condon et al. 1994), and the NRAO-NASA Green Bank Earth Station (Langston et al. 2000), respectively.

[1] The Infrared Processing and Analysis Center (IPAC) is funded by NASA as part of the *IRAS* extended mission under contract to the Jet Propulsion Laboratory.

2.1. *Radio Continuum Data*

Figure 1 shows the 1420 and 408 MHz radio continuum images obtained with the DRAO ST. In both images, the most remarkable structure is a ringlike feature of $\sim 20'$ diameter centered at (J2000) (R.A., decl.) $\sim$ ($19^h58^m.8$, $31°26'.5$) (the "ring" hereafter). The star symbol indicates the position of the Wolf-Rayet star WR 130. There are two OB stars in the field, indicated by plus signs (Stock, Nassau, & Stephenson 1960). Several knots of emission are seen projected on the ring, particularly in the 1420 MHz image, whereas only the brightest component is detected at 408 MHz. We label these sources G68.14+0.92, J1958+3135, J1959+3130, and J1959+3138 (the galactic and extragalactic nature of these sources is confirmed below). Their coordinates are shown in Table 3. Note that the ring is projected on a fainter region of diffuse emission extending in a northeastern to southwestern direction, roughly parallel to the Galactic plane.

In order to study the nature of the ring, the properties of the four point sources must be determined. Since the 408 MHz image is of too low a resolution, we examined images of the same region at other frequencies. These images are shown in Figure 2. At 327 MHz, all four point sources are observed, while only G68.14+0.92 is detected at 2695 MHz and 4.85 GHz. The general shape of the ring is comparable at all frequencies, except at 8.35 GHz where, as a consequence of the lower resolution (a half-power beamwidth of 9.7), only elongated emission is detected. A higher resolution image at 1.4 GHz obtained from the NRAO VLA Sky Survey (NVSS; Condon et al. 1998) is shown in Figure 3. The lack of extended emission is due to the fact that short spacing information is absent in this image. An additional compact source is observed $\sim 1'$ north of WR 130. It consists of two separate components located at (R.A., decl.) = ($19^h59^m11^s.49$, $+31°28'38''.1$) and ($19^h59^m12^s.98$, $+31°27'35''.6$), with flux densities of 6.6 and 9.1 mJy, respectively. The position of WR 130 is (R.A., decl.) = ($19^h59^m12^s.68$, $+31°27'9''.7$). The source is also visible on the DRAO image (Fig. 1), where it appears as a single source of flux density 15 mJy. Its presence on the 327 MHz image at about the same level suggests that it is thermal in nature.

2.2. *Infrared Data*

The 60 and 100 μm images of the same area as above are displayed in Figure 4. The ring is clearly observed at both wavelengths, as well as G68.14+0.92. Two other sources or knots of emission that were not discernible in the radio

TABLE 2

OBSERVATIONAL PARAMETERS FOR VLA DATA

Parameters	H110α RRL at 4.87 GHz	H I 21 cm Line
Right ascension of the field center (J2000).....	19 59 07.6	19 59 08.7
Declination of the field center (J2000)	31 21 02	31 21 42.1
LSR central velocity (km s^{-1})	−32.0	−25.0
VLA configuration	D	DnC, D
FWHM of synthesized beam (arcsec)	12.9 × 12.6	37.7 × 29.6
Position angle (deg)	66	66
Velocity coverage (km s^{-1}).....	192.3 (3125 KHz)	165 (781.25 KHz)
Velocity resolution (km s^{-1})	3.0	1.3
rms noise (mJy beam^{-1}).....	0.7	1.15
Flux density calibrator	3C 48	3C48, 3C 286
Phase calibrator	2023+318	3C 48

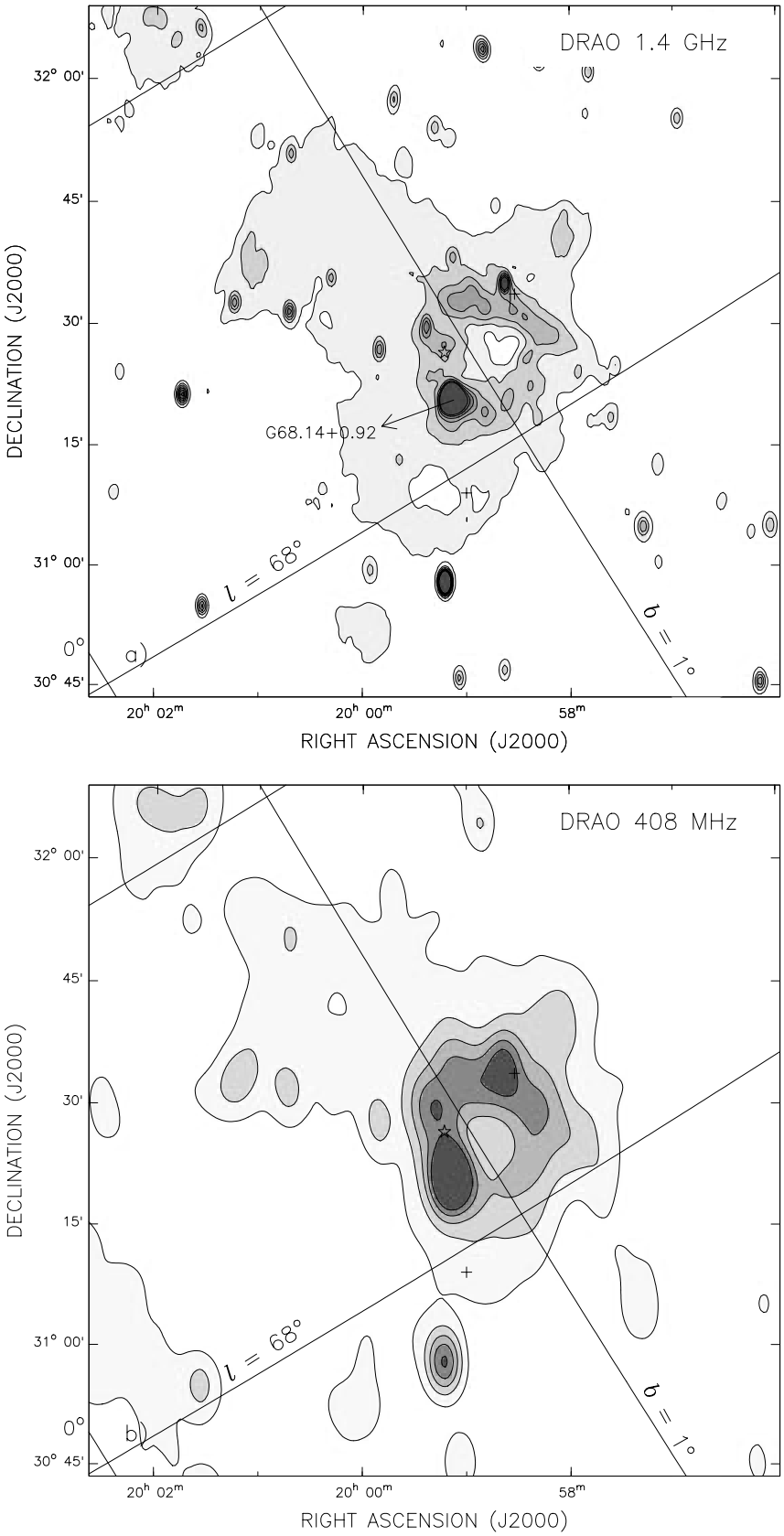

FIG. 1.—Radio continuum images obtained at DRAO. The star symbol indicates the position of WR 130. The plus signs indicate the position of the OB stars. (*a*) 1420 MHz, $(\theta_\alpha \times \theta_\delta) = (1.'0 \times 1.'9)$. Contour levels are at 8–14 K in steps of 1 K. (*b*) 408 MHz, $(\theta_\alpha \times \theta_\delta) = (3.'3 \times 6.'5)$. Contour levels are at 85–125 K in steps of 10 K. In both images, the lines $b = 1°$ and $l = 68°$ are shown.

TABLE 3

FLUX DENSITIES (IN MJY)

Source	R.A. (J2000)[a]	Decl. (J2000)[a]	Major Size[a] (arcsec)	Minor Size[a] (arcsec)	327[b] (MHz)	1420[c] (MHz)	4850[d] (MHz)	α
G68.14+0.92.....	19 59 08.45	31 21 18.1	285.6	139.7	582 ± 30	724 ± 25.5	639 ± 83	−0.03
J1958+3135	19 58 37.65	31 35 39.8	<20.3	<17.5	216 ± 4	66.2 ± 2.0	...	−0.8
J1959+3130	19 59 23.14	31 30 11.8	77.0	20.8	117 ± 5	32.9 ± 2.2	...	−0.9
J1959+3138	19 59 07.74	31 38 54.4	<29.2	<22.6	75 ± 3	14.0 ± 0.7	...	−1.1

[a] NVSS catalog; Condon et al. 1998.
[b] WSRT 327 MHz Galactic Plane Discrete Source Catalog; Taylor et al. 1996.
[c] NVSS catalog; Condon et al. 1998.
[d] 87 GB Catalog of Radio Sources; Gregory & Condon 1991.

images are clearly observed projected on the ring. The images at 12 and 25 μm are not shown here, since the morphology of the ring is comparable to the 60 and 100 μm images.

2.3. H I *Data*

In order to analyze the distribution of the neutral gas around WR 130, we examined the H I emission in the region $19^h52^m.5 < \alpha < 20^h6^m$ and $30^\circ.0 < \delta < 32^\circ.8$. Using the DRAO ST data, we constructed an H I cube with a velocity interval of 1.65 km s^{-1}. For ease of presentation, a constant background corresponding to the average brightness temperature in a radius of 50′ around WR 130 was subtracted from each channel map. The mean subtracted spectrum is shown in Figure 5. After inspecting the whole data cube for structures that could be related to WR 130, we found two

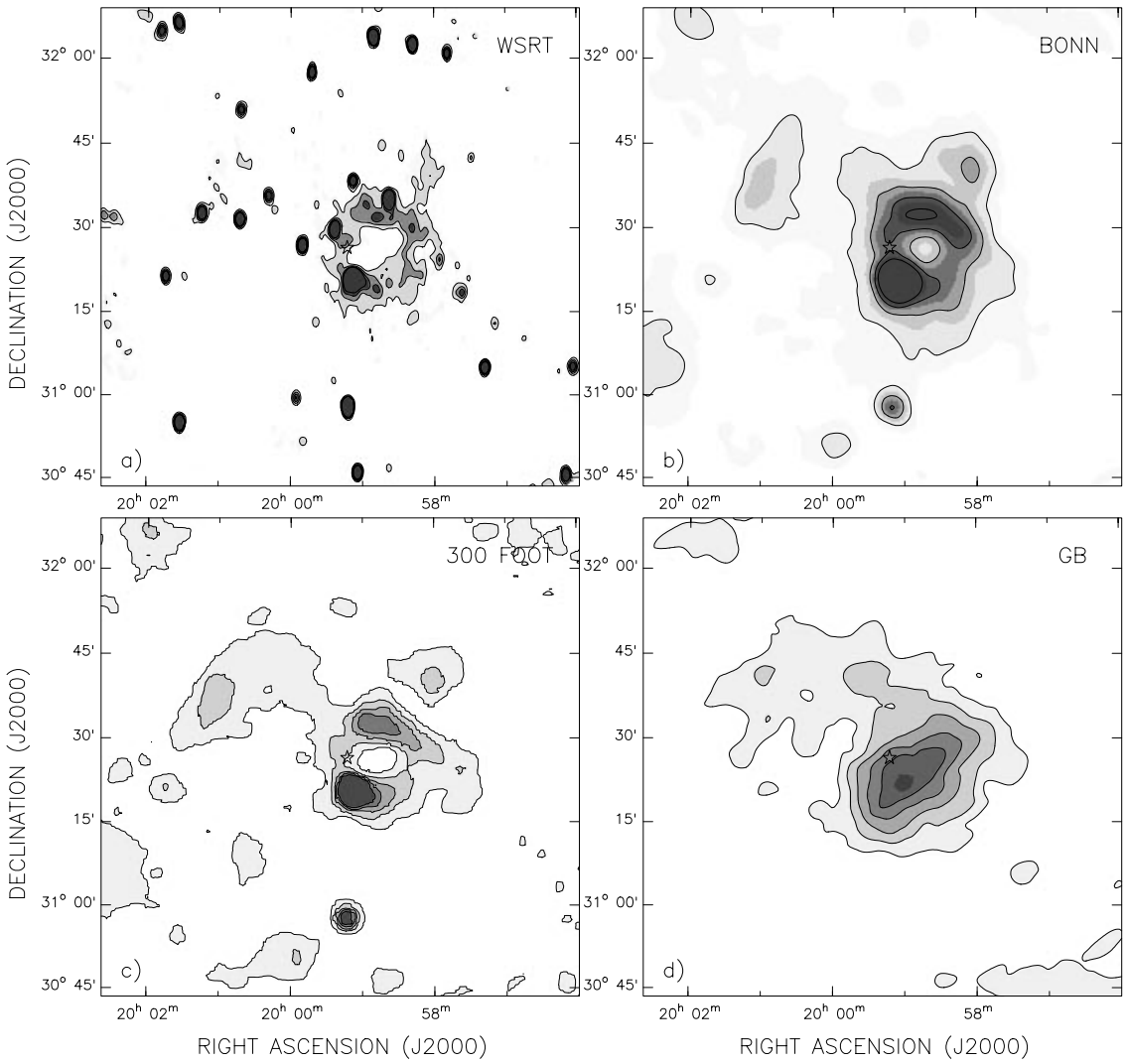

FIG. 2.—Radio continuum images of the same area as in Fig. 1, obtained from various surveys. The star symbol indicates the position of WR 130. (*a*) 327 MHz (Taylor et al. 1996), $(\theta_\alpha \times \theta_\delta) = (1' \times 1'.9)$. Contour levels are at 15–60 K in steps of 15 K. (*b*) 2695 MHz (Fürst et al. 1990), $(\theta_\alpha \times \theta_\delta) = (4'.3 \times 4'.3)$. Contour levels are at 0.2–0.8 K in steps of 0.2 K. (*c*) 4.85 GHz (Condon et al. 1994), $(\theta_\alpha \times \theta_\delta) = (3'.7 \times 3'.3)$. Contour levels are at 0.01–0.17 K in steps of 0.04 K. (*d*) 8.35 GHz (Langston et al. 2000), $(\theta_\alpha \times \theta_\delta) = (9'.7 \times 9'.7)$. Contour levels are at 0.01–0.05 K in steps of 0.01 K.

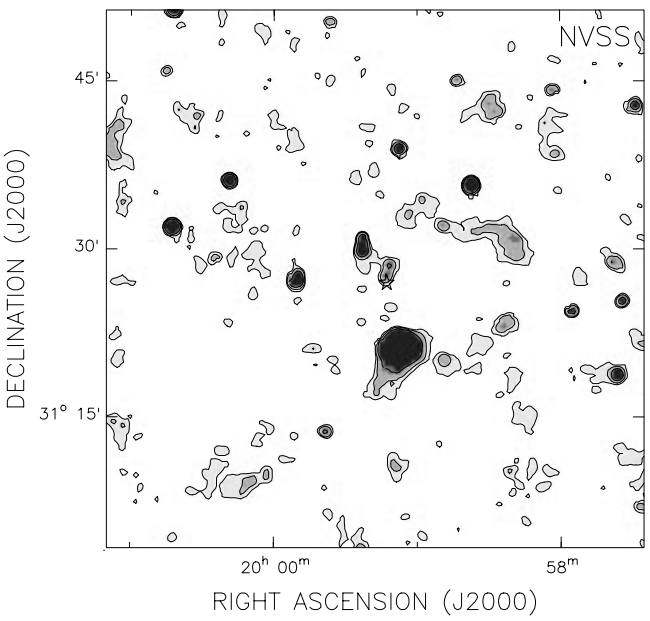

FIG. 3.—A 1.4 GHz radio continuum image from the NVSS survey (Condon et al. 1998). The star symbol indicates the position of WR 130. Resolution is 45″. Contour levels are 1, 2, and 5 mJy beam^{-1}.

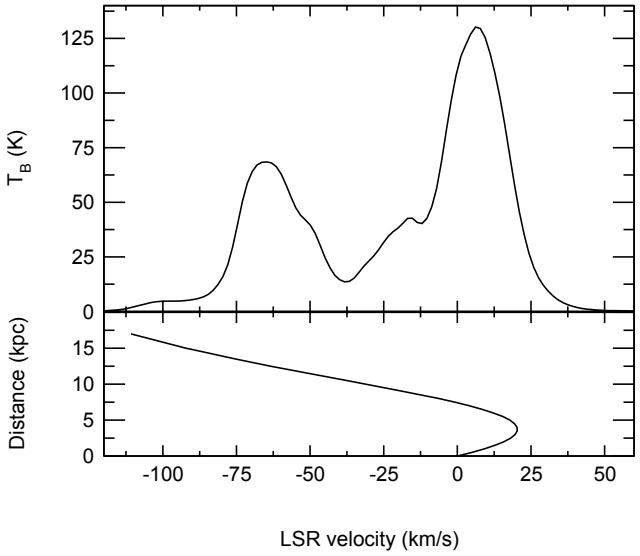

FIG. 5.—Average H I emission spectrum within a circle of 50′ in radius centered at the position of the WR star. The galactic rotation curve given by the model of Fich et al. (1989) is shown in the bottom panel.

significant features at (1) -12 to 1 km s^{-1} and (2) -25 to -33 km s^{-1}.

Figure 6 shows a collection of images spanning the velocity interval -51.2 to 9.1 km s^{-1}. Three channels are averaged to provide an effective resolution of 5.9 km s^{-1}. The images have been smoothed to a resolution of 3′.

Inspection of these images reveals the presence of a minimum in the H I distribution centered at (R.A., decl.) = ($19^h58^m.5$, 31°26′) between 4 and -16.5 km s^{-1} (Figs. 6*b*–6*e*). This cavity is best defined in Figure 6*c*, and it is partially present in Figures 6*b* and 6*e*. The WR star is located at the east border of the cavity.

Another low-emission H I region is observed within the velocity interval -25 to -36 km s^{-1}. This H I minimum has an elongated shape extending toward the northeast, with the WR star appearing projected against the southern part. There is no evidence for radio continuum or IR counterparts. The kinematical distance of this structure is about 9 kpc (Fich, Blitz, & Stark 1989), which is not compatible with the distance of the WR star (see § 1). For these reasons, this feature is not considered further in this paper.

2.4. *Recombination Line Data*

Using the VLA, the H110α recombination line at 4.87 GHz was observed in the direction of G68.14+0.92 at

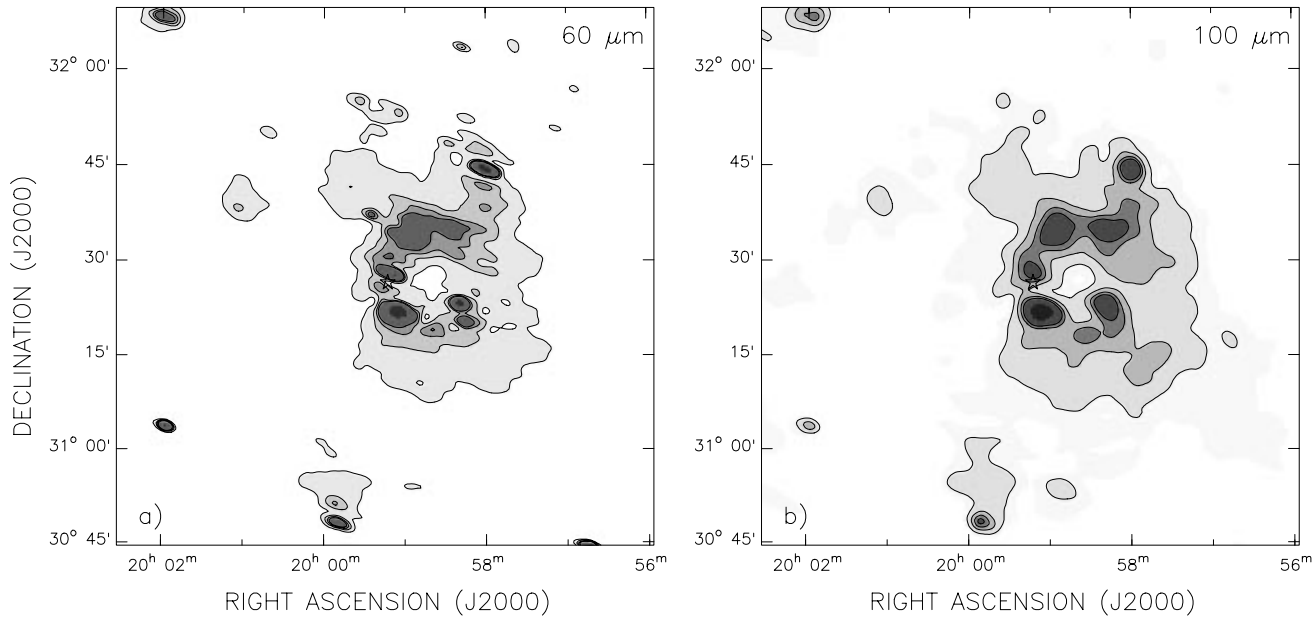

FIG. 4.—HIRES maps of the same area as in Fig. 1. The star symbol indicates the position of WR 130. (*a*) 60 μm. Resolution (slightly variable over the map) is 1.′62 × 1′ at a P.A. of 154° east of north. Contour levels are 15–60 MJy sr^{-1} in steps of 15 MJy sr^{-1}. (*b*) 100 μm. Resolution is 2.′12 × 1.′83 at a P.A. of 150° east of north. Contour levels are 50–170 MJy sr^{-1} in steps of 40 MJy sr^{-1}.

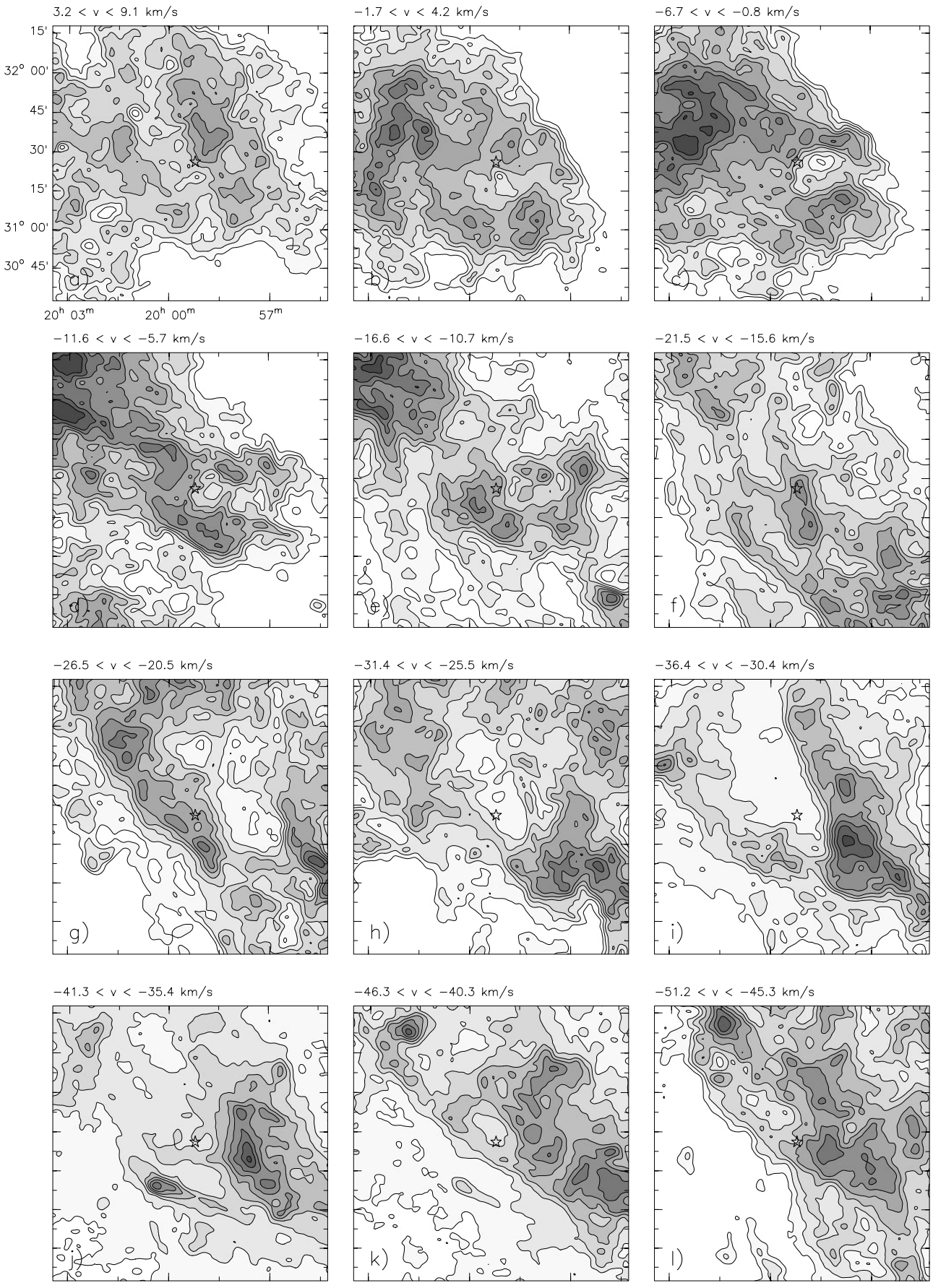

FIG. 6.—DRAO gray-scale images showing the H I gas distribution in the velocity range 9.1 to -51.2 km s^{-1}. The position of WR 130 is indicated by a star symbol. Velocity resolution is 4.9 km s^{-1}, and spatial resolution is 3′. The velocity interval of each image is indicated in the top left corner. Contour levels are -10 to 30 K in steps of 5 K.

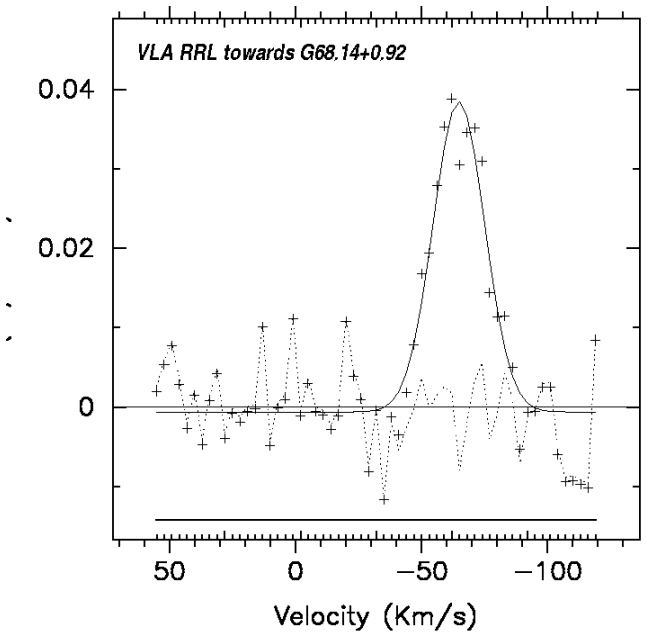

FIG. 7.—Spatially integrated, continuum-weighted H110α line profile toward G68.14+0.92 obtained with the VLA at 4.87 GHz. Resolution is ~13″ and 3.0 km s^{-1}. Data points (*plus signs*), model curve (*solid line*), and residuals (*dotted line*) are shown.

(R.A., decl.) = ($19^h59^m7^s.6$, 31°21′2″) (J2000). Based on a Gaussian fit to the observed profile (see Fig. 7), we deduce a central line velocity of -64.8 ± 2.0 km s^{-1}, a line-to-continuum ratio of 0.039 ± 0.005, and a line width (FWHM) of 24 ± 4 km s^{-1}. From these values, an LTE electron temperature, T_e^*, of 9800 ± 1000 K is obtained assuming a singly ionized helium abundance, Y^+, of 0.1 (Roelfsema & Goss 1992).

3. RESULTS

3.1. *Nature of the Radio Continuum Emission*

To elucidate the nature of these sources and their possible relationships, we have analyzed the available continuum data. As mentioned in § 2.1, two main continuum features are observed toward WR 130: (1) a strong compact source (G68.14+0.92) located a few arcminutes south of the WR star and (2) an outstanding ringlike feature.

3.1.1. *Compact Sources*

The available cataloged flux densities and spectral indexes for the brighter compact sources are listed in Table 3. The value obtained for G68.14+0.92 is typical for an H II region, while the others are representative of extragalactic nonthermal radio sources. Figure 8 is a high-resolution 4.87 GHz VLA radio image of G68.14+0.92. A prominent break in the northeastern edge is observed.

3.1.2. *Ringlike Source*

Three different methods were used in order to determine the nature of this source: calculations of the spectral index were made using (1) integrated radio flux densities, (2) the *T-T* plot method, and (3) the correlation between the radio and the infrared continuum emission.

1. *Integrated radio spectrum.* To obtain the flux density of the ring at each frequency, the diffuse emission associated with background and foreground sources was first subtracted. Because of the presence of a diffuse and varying background, an accurate determination of the true size of the extended emission is difficult. For this reason, we measured the flux densities using different areas and used the different values obtained to infer the flux density uncertainty. The flux density values of the bright point sources discussed above were also subtracted. The resultant radio spectrum is shown in Figure 9. The best fit of these values gives a spectral index for the ring of $\alpha = 0.0 \pm 0.1$, the value expected for thermal free-free emission.

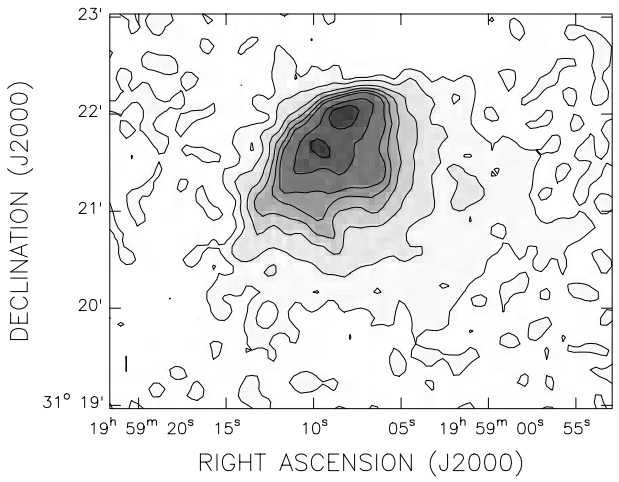

FIG. 8.—A 4.87 GHz VLA radio image of G68.14+0.92. Resolution is ~13″. Contour levels are at 0, 1, 3, 5, 7, 9, 15, and 20 mJy beam^{-1}.

2. *Spectral index from the T-T plot method.* In order to obtain an independent spectral index determination for the ring, we made a so-called *T-T* plot, in which the brightness temperature at one frequency is plotted point by point against the brightness temperature at another frequency. The spectral index is derived from the slope of the fitted straight line (see, e.g., Pineault et al. 1997). This method has the advantage that the spectral index does not depend on the background, as long as the latter varies smoothly. We used the 327 and 1420 MHz images, in which the brighter

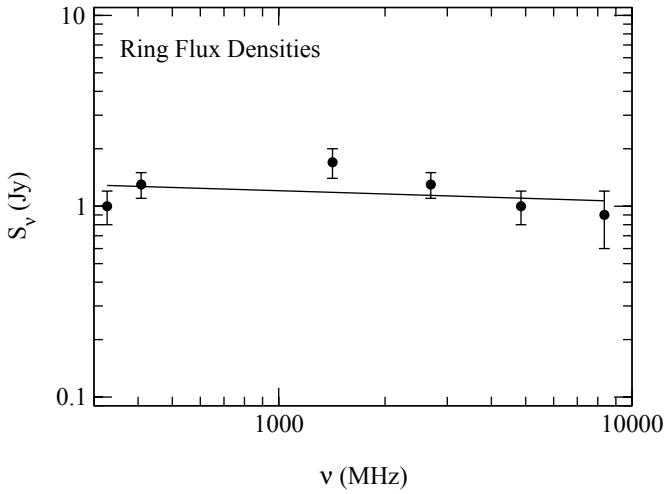

FIG. 9.—Radio spectrum of the ring based on integrated flux densities. The straight line is a least-square fit to the data at 327, 408, 1420, 2695, 4850, and 8350 MHz. It corresponds to $\alpha = 0.0 \pm 0.1$ where $S_\nu \sim \nu^\alpha$.

point sources are resolved, since it is then possible to define an area (inside which the T-T plot is done) that excludes these sources. From images convolved to a common resolution of $2' \times 2'$, we obtained the T-T plot and best-fit line as shown in Figure 10. The corresponding spectral index is $\alpha_{tt} = 0.2 \pm 0.1$.

3. *Correlation between radio continuum and infrared emission.* For H II regions, a strong correlation exists between the brightness temperature at 11 cm, $T_{b,11}$, and I_{60}, its equivalent at 60 μm (Broadbent, Haslam, & Osborne 1989; Moon & Koo 1994). Broadbent et al. (1989) obtained the relation $T_{b,11} = (6.4 \pm 1.7) \times 10^{-3} I_{60}$, where $T_{b,11}$ is in K and I_{60} in MJy sr^{-1}. On the other hand, $T_{b,11} = 0.26 \times T_{b,21}$, assuming a spectral index of $\alpha = -0.1$; thus, we infer that $T_{b,21} = (24.6 \pm 6.5) \times 10^{-3} I_{60}$. In order to test this correlation, the 1420 MHz and 60 μm images were first convolved to a common resolution of $2' \times 2'$. Figure 11 is a plot of $T_{b,21}$ against I_{60}. We fitted two lines, considering the points associated with the ring and the H II region G68.14+0.92. The derived slopes are 0.023 ± 0.001 and 0.035 ± 0.003, respectively. These values are consistent with the slope expected for an H II region.

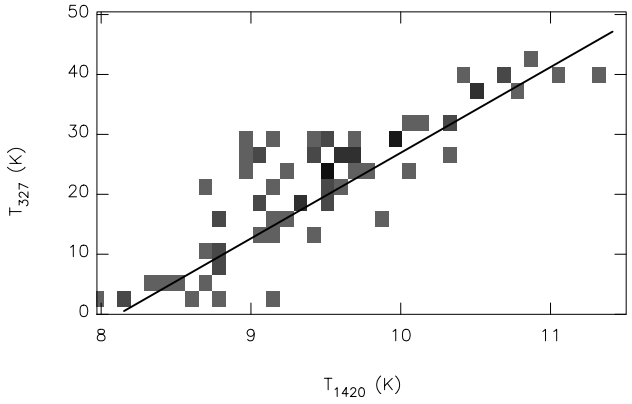

FIG. 10.—T-T plot obtained from the 327 (WSRT) and 1420 (DRAO) MHz data. The fitted line yields a value of $\alpha = 0.2 \pm 0.1$.

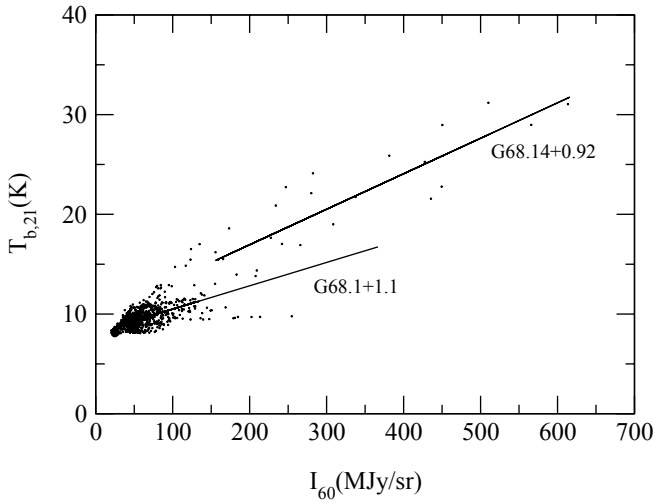

FIG. 11.—The 21 cm continuum brightness temperature, $T_{b,21}$, vs. 60 μm intensity, I_{60}. Solid lines are fits obtained for G68.14+0.92 and the ring (G68.1+1.1).

In summary, all evidence suggests that the ring, which we shall designate G68.1+1.1, has a thermal spectrum.

3.2. *Physical Parameters of the Radio Continuum Sources*

We use the models of Mezger & Henderson (1967) to infer the properties of G68.14+0.92 and G68.1+1.1. From the measured total flux density S_ν, the measured half-power Gaussian width (after correction for the beam) θ_{Ga}, the electron density n_e, mass of ionized gas $M_{H\,II}$, and total number N_u of UV ionizing photons needed to keep the source ionized (see, e.g., Chaisson 1976) can be derived.

The H II region parameters depend weakly on the temperature, which for simplicity we take as $T_e = 10{,}000$ K for both sources (see § 2.4). As for the distances, d, adopted in this section (5 kpc for G68.1+1.1 and 12 kpc for G68.14+0.92), they are discussed at length and justified in § 4.1.

3.2.1. *Compact* H II *Region G68.14+0.92*

The relevant parameters for the compact H II region G68.14+0.92 have been derived, adopting $S_{1420} = 0.7$ Jy, $\theta_{Ga} = 2'.5$, and $d = 12$ kpc. We obtain an electron number density $n_e \sim 35$ cm^{-3} and an ionized mass of $\sim 700\ M_\odot$. The corresponding maximum emission measure (Mezger & Henderson 1967) is $\sim 12{,}000$ pc cm^{-6}. Table 4 lists some of the parameters derived for this source.

3.2.2. *Ringlike* H II *Region G68.1+1.1*

The geometry of G68.1+1.1 can be defined by assuming that the ionized gas is present in a shell of inner and outer Gaussian widths, θ_i and θ_o, respectively. Hence, the term $\theta_{Ga}^{1.5}$ should be replaced by $(\theta_o^3 - \theta_i^3)^{1/2}$. Using the measured flux density at 1420 MHz, values of $7'.5$ and $19'.5$ for θ_i and θ_o, and $d = 5$ kpc, we have calculated the physical parameters for a spherical source model. In the terminology of Mezger & Henderson (1967), this corresponds to a uniform electron density. The derived parameters are presented in Table 4.

We determine the approximate emission measure, E_{ff}, of the ring. The brightness temperature due to optically thin free-free emission, T_{ff}, is given by $T_{ff} = T_e \tau_{ff}$, where τ_{ff} is the

TABLE 4

DUST AND GAS PARAMETERS FOR G68.14+0.92 AND G68.1+1.1[a]

Parameters	G68.1+1.1[b]	G68.14+0.92
Assumed distance (kpc).....	5	12
Ionized gas:		
$M_{H\,II}/M_\odot$	3000	700
n_e (cm^{-3})	3	35
N_u (10^{47} s^{-1}).....	33	80
Dust:[c]		
T_d (K)	34	31
$I_{IR}/L_\odot$	5.1×10^4	6.1×10^4
$M_d/M_\odot$	7	19
Neutral gas:		
$M_{H\,I}^{miss}/M_\odot$	500	...
$M_{H\,I}^{sh}/M_\odot$	1450	...
n_H (cm^{-3}).....	4	...

[a] $M_{H\,II} \propto d_{kpc}^{2.5}$, $n_H \propto d_{kpc}^{-1}$, and $T_d \propto d_{kpc}^{0}$, and all other parameters are $\propto d_{kpc}^{2}$.

[b] Without the four brightest compact sources.

[c] Emissivity parameter $n = 1.5$ ($\kappa_\nu \propto \nu^n$, normalized to 40 cm^2 g^{-1} at 100 μm).

free-free optical depth; the latter is given by (see, e.g., Mezger & Henderson 1967; Chaisson 1976) $\tau_{\rm ff} = 3.2 \times 10^{-7} a T_4^{-1.35} \nu_{\rm GHz}^{-2.1} E_{\rm ff}$, where $\nu_{\rm GHz}$ is the frequency in GHz, T_4 the temperature in units of 10^4 K, a is the Gaunt factor, and the emission measure $E_{\rm ff}$ is in pc cm^{-6}. In the well-defined parts of the ring, the excess brightness temperature over the background is about 2–2.5 K, corresponding to an excess emission measure of 1300–1600 pc cm^{-6}, respectively. Taking the optical extinction in this direction (van der Hucht 2001) as $A_V \approx 6$ mag, we conclude that the optical emission measure is lower by a factor of the order of 250, hence explaining the lack of clearly visible ring structure.

3.3. *Infrared Parameters*

Table 5 is a summary of the infrared flux densities measured in the four *IRAS* wavebands for the different sources and the associated colors. Following Chan & Fich (1995), we can also calculate a total integrated infrared luminosity as $L_{\rm IR}/L_\odot = 1.58 F d_{\rm kpc}^2$, where F is the integrated flux in janskys, given by $F = 1.3(F_{12} + F_{25}) + 0.7(F_{25} + F_{60}) + 0.2(F_{60} + F_{100})$, and where the subscripts are the infrared wavelengths in microns. The final step is to estimate the total amount of radiatively heated dust. Using the 60 and 100 μm data and standard dust grain parameters (Draine & Lee 1984), the dust temperature and mass can be written as (see, e.g., Draine 1990; Dwek & Arendt 1992; Whittet 1992)

$$T_d = (95.94/\ln B_n)\ {\rm K}\ ,$$

$$M_d/M_\odot = m_n F_{60} d_{\rm kpc}^2 (B_n^{2.5} - 1)\ ,$$

where $B_n = 1.667^{3+n} F_{100}/F_{60}$ and the fluxes are in janskys. The parameter n is related to the dust absorption efficiency ($\kappa_\nu \propto \nu^n$, normalized to 40 cm^2 g^{-1} at 100 μm). For the value of n adopted ($n = 1.5$), $m_{1.5} = 0.30 \times 10^{-6}$. The results of the various computations are presented in Table 4.

3.4. H I *Features*

In order to analyze in more detail the H I structure detected at low velocities (see § 2.3), we present (Fig. 12) a set of images showing the H I distribution in the velocity interval 1.2 to -12.0 km s^{-1}, with a velocity separation of 1.65 km s^{-1}.

Although the H I gas distribution along the line of sight to WR 130 shows a complex spatial structure, a feature possessing the characteristics expected from a star with a stellar wind is observed in the vicinity of the WR star. Based on the image at 1.2 km s^{-1}, the WR star is projected onto an extended region of relatively low H I emissivity. This region is first defined at the velocity of -0.43 km s^{-1}, where this H I hole appears centered at (R.A., decl.) $\sim$ ($19^{\rm h}58^{\rm m}$, $+31°25'$) and becomes the dominant feature in the neighborhood of WR 130 from -2.1 to -8.7 km s^{-1}. The WR star is observed projected close to the inner border of the H I shell that surrounds the minimum. This surrounding H I shell is patchy and opens to the west. At velocities more negative than -13 km s^{-1}, this H I feature is not obvious. Figure 13*a* shows the mean brightness temperature image within the velocity range $v \sim -8.4$ to 1 km s^{-1}. The cavity is striking, and the WR star lies at the border, approximately 6′ from the geometrical center.

In order to compare this cavity with the ring observed in the continuum, Figure 14 shows the image of the H I distribution (*gray scale*) and the 1420 MHz continuum emission (*contours*). The physical agreement between the ring and the H I cavity is excellent, indicating that both features are quite likely physically related.

A number of parameters characterizing this H I structure can be derived. Assuming the gas is optically thin, the neutral masses can be easily obtained. Following the procedure described by Pineault (1998), at a distance of d kpc, an H I feature of angular size $\Omega_{\rm am2}$ arcmin^2 and a mean velocity width of Δv km s^{-1} has a mass given by

$$M_{\rm H\,I}/M_\odot \approx 1.3 \times 10^{-3} d_{\rm kpc}^2 \Delta v \int \Delta T_B\, d\Omega_{\rm am2}\ .$$

The above equation being an approximation to an exact integral over velocity, we simply take Δv as the velocity width over which the H I bubble is most visible, namely $\Delta v \sim 10$ km s^{-1} (e.g., Fig. 12).

Since we need to derive the missing H I mass in the cavity ($M_{\rm H\,I}^{\rm miss}$) and the excess H I mass in the shell ($M_{\rm H\,I}^{\rm sh}$), we define three different temperatures: T_c as the average brightness temperature in the cavity, $T_{\rm bg}$ as the background temperature, and T_s as the average brightness temperature in the shell. To obtain $M_{\rm H\,I}^{\rm miss}$ and $M_{\rm H\,I}^{\rm sh}$, we use $\Delta T_B^{\rm miss} = (T_c - T_{\rm bg})$ and $\Delta T_B^{\rm sh} = (T_s - T_{\rm bg})$.

As can be seen from Figure 13*a*, the nonuniform background makes the determination of the shell location difficult. Nevertheless, by smoothing this image to a 30′ resolution and subtracting it from the 3′ resolution image, we obtained the image shown in Figure 13*b*. Since the large-scale structures are absent, the shell position is now delineated. Using the above equation and taking $T_c = 0$ K, $T_{\rm bg} = 5$ K, $T_{\rm sh} = 10$ K, $\Delta v = 10$ km s^{-1}, and $d = 5$ kpc, we obtain $M_{\rm H\,I}^{\rm miss} \sim 500\ M_\odot$ and $M_{\rm H\,I}^{\rm sh} \sim 1450\ M_\odot$. If we assume that the cavity is a spherical volume of radius $r = (\Omega/\pi)^{0.5} d$,

TABLE 5

IRAS Flux Densities and Colors

	Flux Density[a] (Jy)				IR Color[b] $C_{i,j}$		
Object	12	25	60	100	12, 25	25, 60	60, 100
G68.1+1.1[c]	80	176	1022	1960	0.86	1.9	0.71
G68.1+1.1[d]	72	142	733	1281	0.73	1.8	0.61
G68.14+0.92.....	3.7	15	173	397	1.5	2.6	0.90

[a] Wavelengths in microns.
[b] IR colors defined as $C_{i,j} = 2.5 \log (F_j/F_i)$.
[c] Entire emission from within the ring.
[d] As above, but excluding emission from the four brightest compact sources.

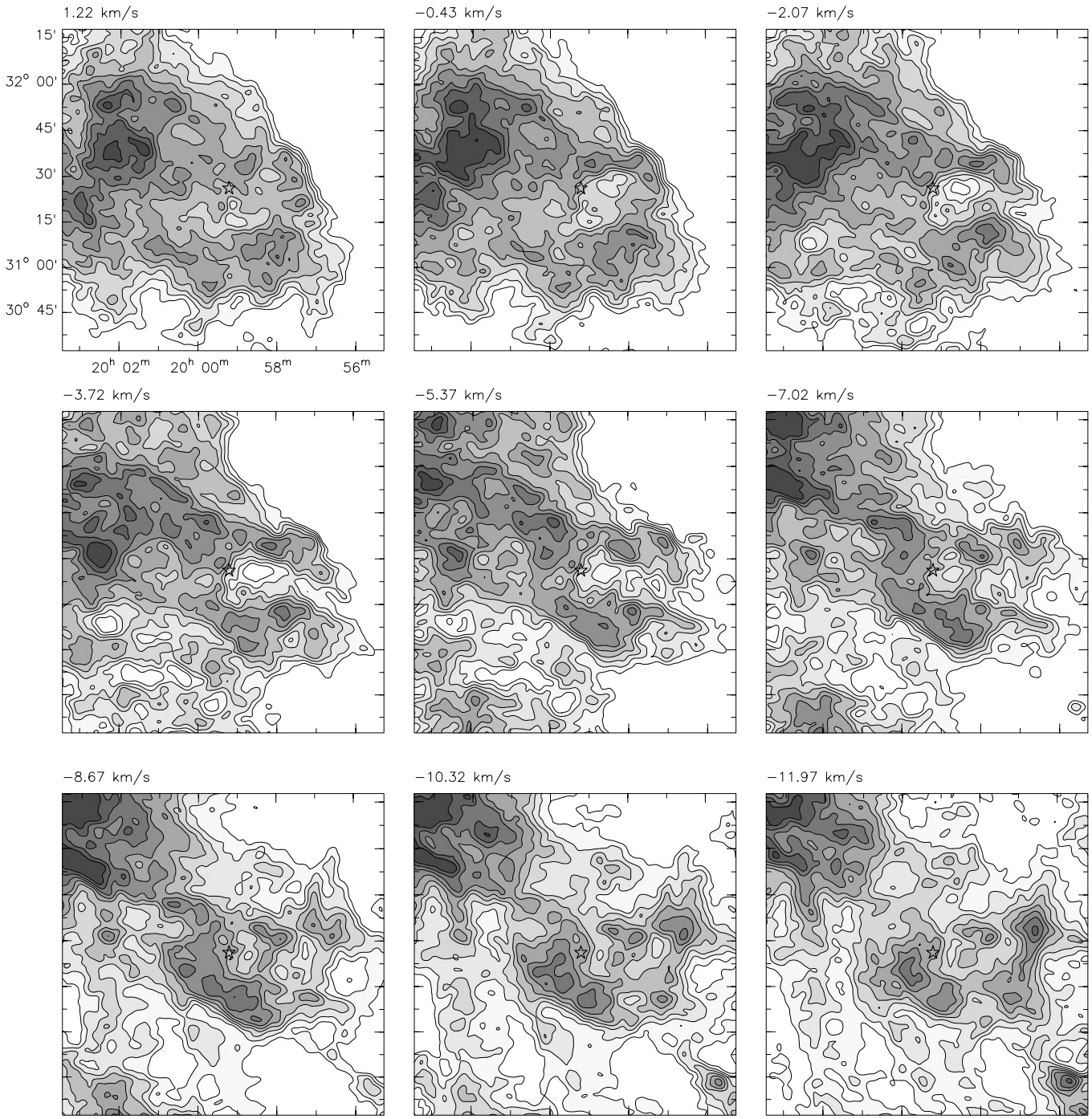

FIG. 12.—DRAO gray-scale images showing the H I gas distribution in the velocity range 1.22 to −11.97 km s^{-1}, with a velocity resolution of 1.65 km s^{-1}. Images have been smoothed to a resolution of 3′. The central velocity of each map is indicated in the top left corner. The star symbol indicates the position of WR 130. Contour levels are −10 to 30 K in steps of 5 K.

we can obtain a lower limit for the neutral gas number density before the gas was ionized and/or swept up in the shell:

$$n_{\rm H}({\rm cm}^{-3}) = 5500(M_{\rm H\,I}^{\rm miss}/M_{\odot})\Omega_{\rm am2}^{-1.5} d_{\rm kpc}^{-3}\ .$$

The derived $n_{\rm H}$ is ~ 4 cm $^{-3}$. The H I results are summarized in Table 4.

4. DISCUSSION

4.1. *Distance to the Sources*

A number of recombination lines have been detected in the field containing G68.14+0.92 and G68.1+1.1. The main parameters are summarized in Table 6. From these data, two mean velocities have been derived, $v \sim -63$ and $v \sim 0.8$ km s^{-1}. A combination of widely differing central coordinates and instrumental resolution may explain the detection or nondetection of the above lines by a given instrument.

Using the VLA H I line data (a beam of $\sim 33''$), an absorption profile toward G68.14+0.92 was obtained (Fig. 15*a*). This spectrum shows a strong absorption feature due to local hydrogen at 0 km s^{-1} and other absorption lines at

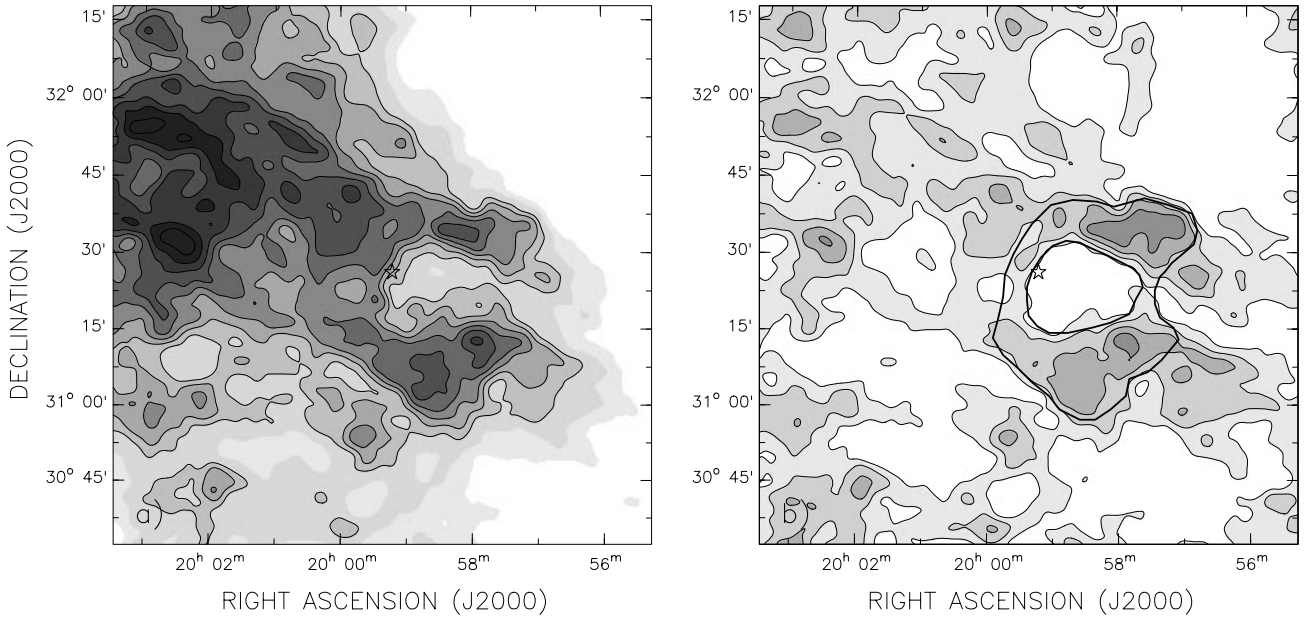

FIG. 13.—(*a*) Average H I emission within the velocity interval −10.3 to 1.2 km s^{-1}. The star symbol indicates the position of WR 130. Contour levels are at 0–28 K in steps of 4 K. (*b*) Same as (*a*) after removing the large-scale structures as described in § 3.4. Contour levels are at 0–20 K in steps of 5 K. The areas used to define the cavity and shell areas are displayed as thick contours.

several velocities out to approximately −65 km s^{-1}. The feature at −65 km s^{-1} allows us to derive a lower limit to the kinematical distance of G68.14+0.92 of about 12 kpc, using the galactic rotation model of Fich et al. (1989). This value is consistent with the recombination line velocity of −64.8 km s^{-1} (see § 2.4). Figure 15*b* shows the absorption spectrum obtained by summing the contribution from three likely extragalactic sources (J1958+3135, J1959+3130, and J1959+3127). The extragalactic source spectrum has many of the same H I features as G68.14+0.92. However, there is excess H I absorption in the range −65 to −80 km s^{-1} arising from H I in the outer galaxy at distances of 12–15 kpc. These velocities are consistent with the extragalactic nature of these three sources. In addition, the DRAO H I full-resolution images (a beam of $\sim 1' \times 2'$) show a clear H I absorption feature in the range +12 to −23 km s^{-1} and −45 to −68 km s^{-1}. The H I size matches the angular extent of G68.14+0.92. In addition, the molecular line CS (2 → 1) (Bronfman, Nyman, & May 1996) has been detected toward G68.14+0.92 (see Table 6) at a velocity of −62.6 km s^{-1}, in agreement with our H110α VLA observations (§ 2.4). Based on the above, we believe that all spectral features observed from −62 to −68 km s^{-1} originate either in the ionized gas or the molecular cloud associated with the compact H II region G68.14+0.92 at a distance of 12 kpc.

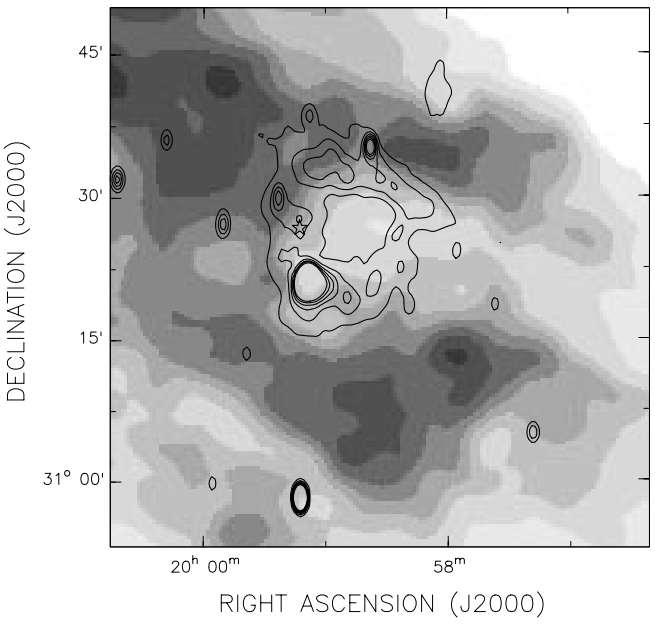

FIG. 14.—Radio continuum contours at 1420 MHz superposed on the H I emission (*gray scale*) from Fig. 13*a*. The star symbol indicates the position of WR 130. Contours are at 9–14 K in steps of 1 K.

As for the recombination lines detected between −2 and 3 km s^{-1}, they arise from the ringlike H II region G68.1+1.1. Inspection of the Digitized Sky Survey (Lasker et al. 1990) shows a good morphological agreement between the faint annular optical emission and the radio continuum ring, thus confirming that G68.1+1.1 is the radio counterpart of the optical H II region Sh 98. Using different galactic rotation models (see, e.g., Fich et al. 1989; Clemens 1985) and the observed velocity field given by Brand & Blitz (1993), we conclude that the gas contributing to the emission observed between −2 to +3 km s^{-1} is located at a far kinematical distance ranging from 5.5 to 7.5 kpc from the Sun. For the sake of completeness, the behavior of the kinematical distance toward $l = 68°$ given by the model of Fich et al. (1989) is shown at the bottom of Figure 5. A similar distance is inferred from our neutral hydrogen observations. The distance of the WR star lies in the range from 2.6 to 4.9 kpc. Bearing in mind the uncertainty in the absolute magnitude of the WR stars, typically ±0.5 mag, it seems reasonable to adopt 5 kpc as the probable distance to both the ring structure and the star.

TABLE 6

RECOMBINATION AND MOLECULAR LINE OBSERVATIONS

Line	R.A. (J2000)	Decl. (J2000)	Beam	Amplitude	V_{LSR} (km s^{-1})	FWHM (km s^{-1})
H125α[a]	19 59 07.7	31 21 03	9′	8 ± 1.4 mK	-62.9 ± 2.6	16.6 ± 3.6
H127α[a]	19 59 07.7	31 21 03	9′	10 ± 1.1 mK	-2.1 ± 2.4	23.8 ± 3.3
Hα[b]	19 59 08.5	31 21 14	2′	11.0 ± 0.3	2.8 ± 0.5	37.1 ± 1.0
H165α[c]	19 58 51.6	31 24 59	36′	11 mK	1.8	20.2
CS (2–1)[d]	19 59 08.5	31 21 47	39″	0.38 K	−62.6	2.9
H110α[e]	19 59 07.6	31 21 02	12″.7	0.04 ± 0.005	-64.8 ± 0.8	24 ± 2

[a] From Lockman 1989.
[b] From Fich, Treffers, & Dahl 1990, relative units.
[c] From Heiles, Reach, & Koo 1996.
[d] From Bronfman et al. 1996.
[e] From this paper, line-to-continuum ratio.

4.2. *Compact* H II *Region G68.14+0.92*

We have argued above that this source is at a distance of the order of 12 kpc. Table 4 shows that $N_u \sim 8 \times 10^{48}$ s^{-1}, which corresponds approximately to the UV luminosity from an O7–O8 main-sequence star ($\sim 10^{49}$ s^{-1}; Vacca, Garmany, & Shull 1996). With an angular size of 2′.5, the linear extent is 8.7 pc and the IR luminosity is 6.1×10^4 $L_\odot$, in agreement with an O7–O8 star. The dust mass is $M_d \sim 20\ M_\odot$, compatible with the derived ionized gas mass of 700 $M_\odot$ if the gas-to-dust ratio is about 35.

4.3. *Origin of G68.1+1.1 and the* H I *Shell*

In this section, we attempt to construct a self-consistent model of the ISM observed in the direction toward WR 130. We first argue that the observed structures can be explained by the action of either WR 130 or the northernmost OB star cataloged by Stock et al. (1960) or both (we disregard the second OB star, since its angular offset from G68.1+1.1 is much larger). We then demonstrate that either a significant space velocity and/or projection effects can explain the noncentral positions.

Considering first the WR star, we note that at a distance of 5 kpc the total UV luminosity required to ionize the ring corresponds to $N_u = 3.3 \times 10^{48}$ s^{-1}. WR 130 is a WN8 star for which the corresponding parameter is estimated as $N_u = 5.0 \times 10^{48}$ s^{-1} (Esteban et al. 1993). The WR star is thus fully able to keep the ring ionized. The derived IR luminosity, 5.1×10^4 $L_\odot$, is also well below the WR star's luminosity of 1.3×10^5 $L_\odot$. A similar calculation can be carried out to see whether the stellar wind of WR 130 could have alone created the bubble and shell structures. We can compare the mechanical energy, E_w, deposited into the ISM during the age of the bubble and the kinetic energy, E_k, of the shell by computing the ratio $\epsilon = E_k/E_w$. The mechanical energy of the wind can be estimated as $E_w = \dot{M} V_w^2\, t/2$, where $\dot{M}$ and V_w are the mass-loss rate and terminal velocity of the wind. The quantity $t = \beta R_s/V_{\rm exp}$ is the dynamical age of the bubble, where $V_{\rm exp}$ is the expansion velocity of the shell and $\beta = 0.5$–0.6 (Koo & McKee 1992), depending on the energetic losses.

We cannot identify any approaching or expanding cap, so that the expansion velocity cannot be found explicitly. However, since the velocity width over which the cavity displays its greatest angular extent is 10 km s^{-1}, it is not unreasonable to take this value as the expansion velocity as well. Furthermore, it is typical of the expansion velocity found for IBs around other WR stars. We adopt $R_s = 14$ pc (which corresponds to the external radius of the ring and to the internal radius of the H I shell) and estimate the age of the bubble as $t \approx 7 \times 10^5$ yr. Using $\dot{M} = (1$–$3) \times 10^{-6}\ M_\odot$ yr^{-1} (see, e.g., van der Hucht 1992; Nugis & Lamers 2000) and $V_w = 1000$ km s^{-1} (see § 1), we obtain $E_w = (0.7$–$2.2) \times 10^{50}$ ergs. Taking an ionized mass in the shell of 3000 $M_\odot$, a neutral mass of 1500 $M_\odot$, and $V_{\rm exp} = 10$ km s^{-1}, we find $E_k = 4.5 \times 10^{48}$ ergs. The ratio ϵ measures the energy conversion efficiency in the bubble. According to current evolutionary models of IBs, $\epsilon \leq 0.2$ (see Koo & McKee 1992). From the above estimate, we derive $\epsilon = 0.02$–0.06. This value of ϵ indicates that the mechanical energy provided by the WR star is more than sufficient to create the observed ring and shell. Similar low values were derived for most of the H I bubbles found surrounding WR and Of stars (Cappa & Herbstmeier 2000; Cappa et al. 1999, and references therein). The age derived for the H I bubble is roughly comparable, within errors, with the duration of the WR phase of a massive star ($\approx 4 \times 10^5$ yr; see Maeder & Meynet 1994), suggesting that G68.1+1.1 was created mainly during the current WR phase. However, the contribution of previous evolutionary phases of the star (RSG or luminous blue variable phases and O star phase) cannot be discarded. Similar ages were found, for example, for the "inner H I shell" related to the ring nebula NGC 6888 (associated with WR 136; Cappa et al. 1996) and for the H I bubble related to WR 143 (Cazzolato & Pineault 2000).

As for the OB star seen projected onto the northwestern side of the ring at $\sim 10'$ from WR 130, its properties are less well known (Stock et al. 1960). We can nevertheless see whether it could alone ionize the ring. From the work of Reed & Nyman (1996) and using $m_{\rm pg} = 12.1$ and a visual extinction of 3.0 mag (a normal extinction at a distance of 5–6 kpc along that line of sight, according to Neckel & Klare 1980), we deduce $M_v = -4.7 \pm 1.1$. The corresponding distance is $4.6^{+3.0}_{-1.9}$ kpc, and the spectral type is O8 to O9 (assuming a main-sequence star). The ionizing flux is then 7.4–3.6×10^{48} s^{-1}, similar to that of the WR star. As for the stellar wind parameters, using the formulae of Lamers & Leitherer (1993) relating the mass-loss rate and the wind terminal velocity to the basic stellar parameters and adopting for these the values given by Vacca et al. (1996), we estimate $L_w \sim 0.3 \times 10^{36}$ ergs s^{-1}. Taken at face value, this luminosity implies that the OB star could contribute significantly. However, if we use the fainter value for the absolute magnitude (-3.6 mag), we deduce that the star is of type B0 to B1. Such a star does not have a powerful enough ionizing flux or stellar wind to create the ring.

We cannot unambiguously rule out the possibility that

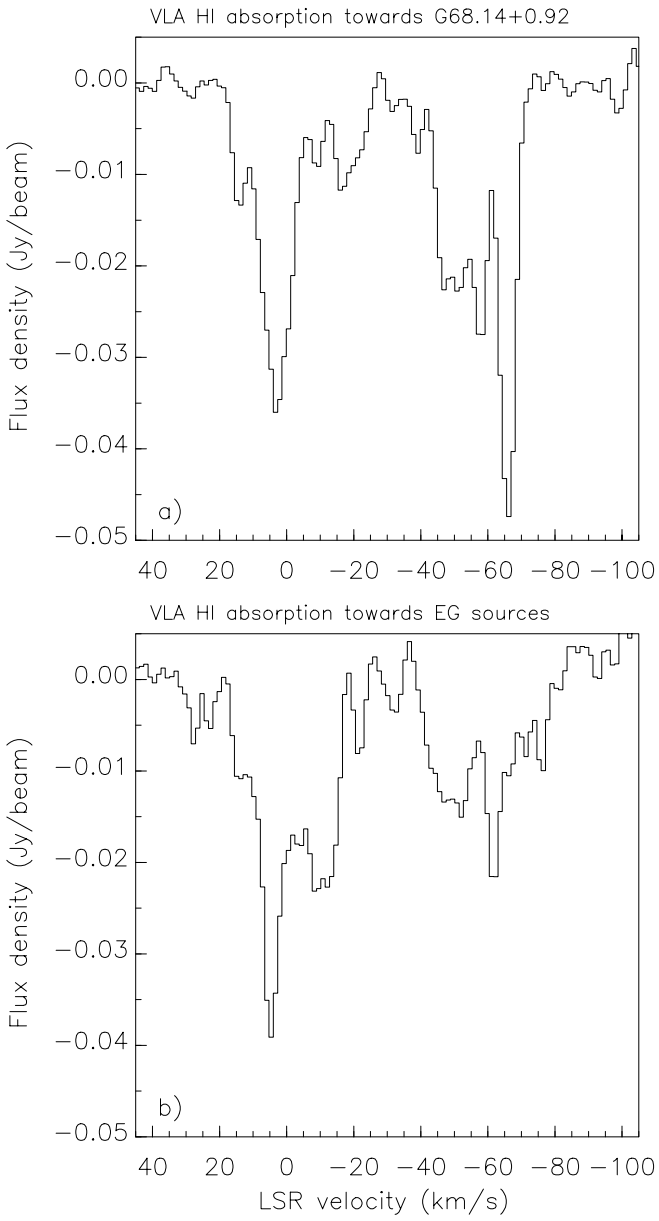

FIG. 15.—Absorption spectra obtained from the VLA H I data (after continuum subtraction). The center of the *u-v* plane was not used (only spacings larger than 1.2 kλ were included). The beam size is $\sim 33''$. (*a*) Mean absorption spectrum toward G68.14+0.92. The continuum level is 47 mJy beam^{-1}. (*b*) Summed absorption spectrum toward three extragalactic sources (J1958+3135, J1959+3130, and J1959+3127). The total continuum level is 30 mJy beam^{-1}.

the OB star contributes to the creation of the observed extended structures. However, given that WR stars are known to be some of the most mechanically powerful stars, it is reasonable to assume that WR 130 is the dominant agent responsible for the extended continuum and H I line features observed.

The position of the WR star at a projected distance of 9 pc from the center of the ring requires an explanation, although this fact does not, in itself, pose a problem. Such a situation has been observed for a number of other WR stars, notably WR 134 (Pineault et al. 1993; Gervais & St-Louis 1999), WR 143 (Cazzolato & Pineault 2000), WR 140 (Arnal 2001), and a number of other stars (Arnal 1992). Among the reasons invoked to explain the asymmetry are a substantial density gradient and/or stellar velocity with respect to the local ISM. However, the case of WR 130 seems more extreme, since the star is seen projected within the walls of the radio and IR continuum ring.

In our opinion, the particular geometry can be explained by a combination of a substantial yet not unreasonable space motion of the star with respect to the local ISM on one hand and the angle that the line of sight makes with the star velocity axis on the other hand. Indeed, the projected noncentral position of the star with respect to the ring center requires a nonzero tangential velocity. The observed 6′ offset of WR 130 with respect to the ring center (corresponding to a separation of 9 pc at a distance of 5 kpc) corresponds to a tangential velocity, v_t, of 18 km s^{-1}, if we assume a reasonable dynamical age of $t \approx 5 \times 10^5$ yr. On the other hand, the apparent absence of interaction in the immediate vicinity of the star suggests that WR 130 is located mostly in front of or behind the major ring structure, possibly in an underdense region, and thus has a substantial radial velocity. As an illustrative case, if the star is moving away from or toward us at an angle of about 30° with respect to the line of sight, the space velocity of the star is then about 40 km s^{-1} and the distance travelled about 20 pc, i.e., about 1.5 times the measured (on the sky) shell radius $R_s \approx 14$ pc. This implies that the three-dimensional bubble created by the star is no longer spherical but has an oblong shape (although its observed appearance can still be quite circular, depending on the viewing direction). Note that this case resembles that which is schematically illustrated in Figure 7 of Weaver et al. (1977), with the very important difference that their illustration shows a star moving in the plane of the sky (i.e., at 90° to the line of sight). The fact that the quoted extinction toward the WR star is about twice that in this general direction suggests that the star is more likely moving away from us and hence is seen through a deeper amount of absorbing material. We note that G68.1+1.1 is not quite perfectly circular and does have some asymmetry. The straighter looking eastern edge of the continuum ring is additional indication that the expanding material is encountering a higher density in that direction.

In a realistic situation, in addition to the space velocity of the star, one would need to take into account the mass-loss history of the current WR star and the possibility that the surrounding ISM is inhomogeneous or shows a substantial density gradient. Nevertheless, we feel that the simple scenario suggested above suffices to justify the association of WR 130 with the extended structures observed in the continuum and line data. This scenario also suggests that more high-resolution observations and a thorough modeling approach are required.

Finally, we see from Table 4 that the mass of ionized gas is substantially higher than that of the neutral gas either observed directly via the 21 cm line or inferred from the IR-emitting dust (for example, if we take the ionized gas and heated dust to coexist in the same volume, the required gas-to-dust ratio is very high). Although this difference can possibly be the result of the difficulty in accurately taking into account the varying background, a simpler explanation may be that the ionized gas present in the ring fills only a fraction f of the ring volume, thus reducing the required mass by a factor of $f^{1/2}$. A filling factor of 0.25 is thus sufficient to lower the ionized gas mass by a factor of 2.

5. CONCLUSIONS

These new radio continuum observations have enabled us to detect a ringlike structure of about 20′ diameter, with the WR star projected onto the ring. The ring, named G68.1 + 1.1, can be identified with the H II region Sh 98, previously suggested to be related to WR 130. The spectral index of the ringlike feature, derived from different methods, indicates a thermal origin. The source also displays a strong correlation between 21 cm brightness temperature and infrared emission, which is typical for H II regions.

An inspection of the DRAO H I images within the LSR velocity interval -12 to 1 km s^{-1} has shown the existence of an H I counterpart to G68.1 + 1.1. The H I images reveal the presence of a minimum in the distribution of neutral gas surrounded by an almost complete envelope. The WR star is close to one of the higher density borders of the surrounding shell. The close morphological agreement between the radio continuum ring and the H I shell indicates that both features are physically related. The structure has a systemic velocity compatible with the velocity of the ionized gas in G68.1 + 1.1 as obtained from radio recombination lines ($\sim$0.8 km s^{-1}). Based on our findings, we conclude that G68.1 + 1.1 and the H I shell are associated with WR 130.

Assuming a distance of 5 kpc for the radio features, the derived inner and outer radius of G68.1 + 1.1 are 5.5 and 14 pc, respectively. The emission measure is in the range 1300–1600 pc cm^{-6}. A comparison of the masses derived from the various components suggests that the ionized material in G68.1 + 1.1 is somewhat clumpy. We note that the UV photon flux from the WR star is able to maintain the ionization of G68.1 + 1.1, and the stellar wind is capable of explaining the bubble and shell structures. Based on evolutionary models of IBs, we estimate a dynamical age of $\leq 7 \times 10^5$ yr, roughly compatible with the WR phase of a massive star. Although this value suggests that G68.1 + 1.1 may have formed during the current WR phase of the star, the contribution of previous evolutionary phases cannot be ruled out.

Consequently, we can interpret the ionized ring and H I shell as the observational manifestation of an IB created by WR 130. The eccentric position of the WR star can be explained by taking into account projection effects, a relatively low stellar velocity ($\leq$40 km s^{-1}), and/or a substantial ambient density gradient. An OB star seen projected on the northwest side of G68.1 + 1.1 cannot be ruled out as a possible contributor to the formation of the structure.

Finally, the derived spectral index of the brightest compact source G68.14 + 0.92 ($\alpha = -0.03 \pm 0.05$) and VLA H110α observations indicate that this source is an H II region located at a distance of about 12 kpc. G68.14 + 0.92 is thus unrelated to either WR 130 or Sh 98. At this distance, the H II region is 9 pc in diameter. The estimated ionized and dust masses are 700 and 20 $M_\odot$. The derived UV photon flux is compatible with an O7–O8 main-sequence exciting star.

E. M. A., C. E. C., S. C., and S. P. are grateful to the staff of the DRAO for their help and warm hospitality during their stay at the observatory. S. C. acknowledges support from the NRAO during her visit to Socorro, New Mexico. One of us (E. M. A.) wishes to thank his colleagues of Université Laval in Quebec for their warm hospitality and for all the attention received during his visit. NRAO is a facility of the National Science Foundation operated under cooperative agreement by Associated Universities, Inc. The DRAO ST is operated as a national facility by the National Research Council of Canada. We acknowledge the use of NASA's SkyView[2] facility located at NASA Goddard Space Flight Center. S. C. acknowledges FOMEC for financial support via a scholarship. This work was partially financed by Consejo Nacional de Investigaciones Científicas y Técnicas (CONICET) of Argentina under project PIP-4252/96 and PIP-607/98 and by Fundación Antorchas, Argentina, through project 13622/10. This work was supported by the Natural Sciences and Engineering Research Council of Canada and the Fonds pour la Formation de Chercheurs et l'Aide à la Recherche de Québec. We are grateful to the anonymous referee, whose comments and suggestions led to the improvement of this paper.

[2] See http://skyview.gsfc.nasa.gov.

REFERENCES

Abbott, D. C., Bieging, J. H., Churchwell, E., & Torres, A. V. 1986, ApJ, 303, 239
Arnal, E. M. 1992, A&A, 254, 305
———. 2001, AJ, 121, 413
Avedisova, V. 1972, Soviet Astron., 15, 708
Baars, J. W. M., Genzel, R., Pauliny-Toth, I. I. K., & Witzel, A. 1977, A&A, 61, 99
Brand, J., & Blitz, L. 1993, A&A, 275, 67
Brighenti, F., & D'Ercole, A. 1994, MNRAS, 270, 65
Broadbent, A., Haslam, C. G. T., & Osborne, J. L. 1989, MNRAS, 237, 381
Bronfman, L., Nyman, L.-A., & May, J. 1996, A&AS, 115, 81
Cao, Y., Terebey, S., Prince, T. A., & Beichman, C. A. 1997, ApJS, 111, 387
Cappa, C. E., Dubner, G. M., Rogers, C., & St-Louis, N. 1996, AJ, 112, 1104
Cappa, C. E., Goss, W. M., Niemela, V. S., & Ostrov, P. 1999, AJ, 118, 948
Cappa, C. E., & Herbstmeier, U. 2000, AJ, 120, 1963
Castor, J., McCray, R., & Weaver, R. 1975, ApJ, 200, L107
Cazzolato, F., & Pineault, S. 2000, AJ, 120, 3192
Chaisson, E. J. 1976, in Frontiers of Astrophysics, ed. E. H. Avrett (Cambridge: Harvard Univ. Press), 259
Chan, G., & Fich, M. 1995, AJ, 109, 2611
Clemens, D. P. 1985, ApJ, 295, 422
Condon, J. J., Broderick, J. J., Seielstad, G. A., Douglas, K., & Gregory, P. C. 1994, AJ, 107, 1829
Condon, J. J., Cotton, W. D., Greisen, E. W., Yin, Q. F., Perley, R. A., Taylor, G. B., & Broderick, J. J. 1998, AJ, 115, 1693
Conti, P. S., & Vacca, W. D. 1990, AJ, 100, 431
Draine, B. 1990, in The Interstellar Medium in Galaxies, ed. H. A. Thronson, Jr. & J. M. Shull (Dordrecht: Kluwer), 483
Draine, B., & Lee, H. M. 1984, ApJ, 285, 89
Dwek, E., & Arendt, G. 1992, ARA&A, 30, 11
Esteban, C., Smith, L. J., Vílchez, J. M., & Clegg, R. E. S. 1993, A&A, 272, 299
Fich, M., Blitz, L., & Stark, A. A. 1989, ApJ, 342, 272
Fich, M., Treffers, R. R., & Dahl, G. P. 1990, AJ, 99, 622
Fowler, J. W., & Aumann, H. H. 1994, in Science with High-Resolution Far-Infrared Data, ed. S. Terebey & J. Mazzarella (JPL Publ. 94-5), 1
Fürst, E., Reich, W., Reich, P., & Reif, K. 1990, A&AS, 85, 691
García-Segura, G., & Mac Low, M.-M. 1995, ApJ, 455, 145
Gervais, S., & St-Louis, N. 1999, AJ, 118, 2394
Gregory, P. C., & Condon, J. J. 1991, ApJS, 75, 1011
Hamann, W.-R., Koesterke, L., & Wessolowski, U. 1995, A&A, 299, 151
Haslam, C. G. T., Stoffel, H., Salter, C. J., & Wilson, W. E. 1982, A&AS, 47, 1
Heckathorn, J. N., Bruhweiler, F. C., & Gull, T. R. 1982, ApJ, 252, 230
Heiles, C., Reach, W. T., & Koo, B. 1996, ApJ, 466, 191
Hidayat, B., Supelli, K., & van der Hucht, K. A. 1982, in IAU Symp. 99, Wolf-Rayet Stars: Observations, Physics, and Evolution, ed. C. W. H. de Loore & A. J. Willis (Dordrecht: Reidel), 27
Joncas, G., & Higgs, L. A. 1990, A&AS, 82, 113
Kallas, E., & Reich, W. 1980, A&AS, 42, 227
Kerton, C. R., & Martin, P. G. 2000, ApJS, 126, 85
Koo, B.-C., & McKee, C. F. 1992, ApJ, 388, 93
Lamers, H. J. G. L. M., & Leitherer, C. 1993, ApJ, 412, 771

Landecker, T. L., et al. 2000, A&AS, 145, 509
Langston, G., Minter, A., D'Addario, L., Eberhardt, K., Koski, K., & Zuber, J. 2000, AJ, 119, 2801
Lasker, B. M., Sturch, C. R., McLean, B. J., Russell, J. L., Jenkner, H., & Shara, M. M. 1990, AJ, 99, 2019
Lockman, F. J. 1989, ApJS, 71, 469
Lozinskaya, T. A. 1992, Supernovae and Stellar Wind in the Interstellar Medium (New York: AIP)
Maeder, A. 1990, A&AS, 84, 139
Maeder, A., & Meynet, G. 1994, A&A, 287, 803
Mezger, P. D., & Henderson, A. P. 1967, ApJ, 147, 471
Miller, G., & Chu, Y.-H. 1993, ApJS, 85, 137
Moon, D. S., & Koo, B. C. 1994, J. Korean Astron. Soc., 27, 81
Neckel, Th., & Klare, G. 1980, A&AS, 42, 251
Normandeau, M., Taylor, A. R., & Dewdney, P. E. 1997, ApJS, 108, 279
Nugis, T., & Lamers, H. J. G. L. M. 2000, A&A, 360, 227
Pineault, S. 1998, AJ, 115, 2483
Pineault, S., & Joncas, G. 2000, AJ, 120, 3218
Pineault, S., Landecker, T. L., Madore, B., & Gaumont-Gay, S. 1993, AJ, 105, 1060
Pineault, S., Landecker, T. L., Swerdlyk, C. M., & Reich, W. 1997, A&A, 324, 1152
Reed, B. C., & Nyman, M. A. 1996, PASP, 108, 395
Roelfsema, P. R., & Goss, W. M. 1992, A&A Rev., 4, 161
Sharpless, S. 1959, ApJS, 4, 257
Steigman, G., Strittmatter, P., & Williams, R. E. 1975, ApJ, 198, 575
Stock, J., Nassau, J. J., & Stephenson, C. B. 1960, Luminous Stars in the Northern Milky Way, Vol. 2 (Hamburg-Bergedorf: Hamburger Sternwarte and Warner Swasey Obs.)
Taylor, A. R., Goss, W. M., Coleman, P. H., van Leeuwen, J., & Wallace, B. J. 1996, ApJS, 107, 239
Vacca, W. D., Garmany, C. D., & Shull, J. M. 1996, ApJ, 460, 914
van der Hucht, K. A. 1992, A&A Rev., 4, 123
———. 2001, NewA Rev., 45, 135
van der Hucht, K. A., Hidayat, B., Admiranto, A. G., Supelli, K. R., & Doom, C. 1988, A&A, 199, 217
Weaver, R., McCray, R., Castor, J., Shapiro, P., & Moore, R. 1977, ApJ, 218, 377
Whittet, D. C. B. 1992, Dust in the Galactic Environment (New York: Inst. Phys.), 169
Willis, A. J. 1991, in IAU Symp. 143, Wolf-Rayet Stars and Interrelations with Other Massive Stars in Galaxies, ed. K. A. van der Hucht & B. Hidayat (Dordrecht: Reidel), 265